Generalized Automated Tool for Analysis and Design of Multiphase Coupled Inductor Buck Converters

Rana Asad Ali, Mahmoud Shousha, Martin Haug
MagI³C PU, Würth Elektronik eiSos Group
Garching bei München, Germany
E-Mail: mahmoud.shousha@we-online.de
URL: Würth Elektronik eiSos Group

Acknowledgements

This work has received support from the European Union's Horizon 2020 program, for the project EleGaNT under the Grant Agreement 101004274.

Keywords

«DC-DC converter», «Coupled inductor», «Modelling», «Design», «Multiphase converter», «Paralleling», «Simulation»

Abstract

This paper presents the implementation and validation of a tool for analyzing multi-phase coupled inductor buck converters. In this type of converter, the equivalent inductance seen by each phase changes significantly within one switching cycle and the number of equivalent inductances increases significantly as the number of phases increase. The manual analysis of these converters is prone to errors and using available simulation tools does not result in a symbolic closed-form solution for the equivalent inductance versus the number of phases. The proposed tool not only considers the coupled inductor design with symmetric inductances and coupling coefficients but also the asymmetric design parameters. Moreover, the possibility of specifying the winding directions of the coupled inductor makes it more suitable for practical applications. The tool is benchmarked against simulation and experimental setup by designing three winding symmetric and asymmetric coupled inductors for three phase buck converters. The tool has an error ranging from 0.0288% to 4.661%.

Introduction

With the increasing power demand of low-voltage and high-current systems such as today's microprocessors, single-phase buck converters pose a challenge to meet steady state requirements for efficiency, output voltage ripples, and thermal performance as well as transient requirements such as output voltage deviation and recovery time. In addition, if the transient response is improved by reducing the inductance value, the system's efficiency degrades due to the high current ripples which also result in high output voltage ripples, making such types of converters ill-fitting to the targeted applications. Moreover, to meet the high-current demand of such systems, single-phase buck converters require an inductor with high inductance and saturation current values, which eventually leads to a big solution size. Therefore, multi-phase buck converters (MPBC) are the solution which address the above-mentioned challenges by having multiple buck converters which operate in parallel at a phase shift of $360°/N$, where N denotes the number of phases. In addition to this, each stage carries lower amounts of current in comparison to the total current, which relaxes the component sizing at the expense of a larger number of components. As far as thermal management is concerned, the thermal hot spots are distributed among the number of phases and hence the system efficiency improves. The multiphase buck converter is different from single phase in a way that output ripple current gets reduced in comparison to phase ripple current due to ripple cancellation effect. The effective frequency at the output of MPBC is multiplied by the factor of N, which eases the design of output filter and reduces the output voltage ripples.

Instead of using discrete inductors per phase in MPBC, the coupled inductors could be used in such applications where the steady-state response and dynamic response require separate optimization by controlling the effective inductance, which is possible in integrated or coupled inductors [1]. These converters are known as multi-phase coupled inductor buck converters (MPCIBC).

Previous works [2]-[3] only analyzed two-phase coupled inductor converters without extending the concept to *N*-number of phases. Analysis of four-phase boost and three-phase buck converters were shown in [4]-[5]. The authors did not consider the difference in mutual inductances between phases, assuming a single value in the analysis. In addition, the direction of winding was not covered in their analysis, resulting in the same equivalent inductance value for both cases. The authors of [6] presented the analysis of two phase-coupled inductors but the analysis is only valid for loosely coupled inductors. The authors of [7]-[9] provide a solution for two equivalent inductances only for *N*-number of phases, however as the number of phases increases, the mode of operation increases, and the number of the equivalent inductances increases. The main goal of this paper is to provide a closed form symbolic solution for MPCIBC, covering all modes of operation for any number of phases considering symmetrical design, asymmetrical design, and winding direction of every phase. A tool is developed on MATLAB allowing users to enter their conditions and giving them the symbolic or numerical equivalent inductances and current-slopes per mode within each case.

Modeling of the Coupled Inductor

A coupled inductor is one which contains a single core with more than one coil wound around it. Due to the presence of a common core, the flux links with other windings, unlike in discrete inductors. This flux linkage changes the voltage appearing across each winding within a switching cycle, hence the analysis of multiphase converters with coupled inductors (MPCIBC) differs from a system with discrete inductors. Figure 1 describes that a coupled inductor can be modeled by $L_{1,lk}$, $L_{2,lk}$, L_m and an ideal transformer. $L_{1,lk}$ and $L_{2,lk}$ are known as leakage inductances, and magnetizing inductance is represented as L_m. [8]-[10].

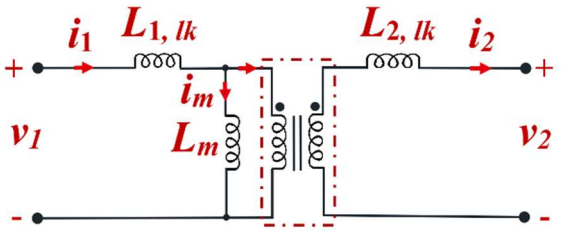

Fig. 1: T model of coupled inductor.

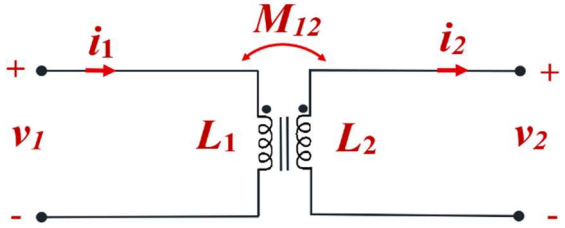

Fig. 2: Modeling of coupled inductor for analysis.

The modelling of the coupled inductor as shown in Fig. 1 is based on leakage L_{lk} and magnetizing inductances. The L_{lk} plays an important role in analysis and operation of power electronics converters such as MPCIBC [8]-[9], [11]. Usually, a short circuit test is performed for measuring the leakage inductance, however, due to high leakage and large air gaps in the magnetic structures of coupled inductors of multiphase converters, it is prone to inaccuracy [12]. Due to this reason, the standard T-model of a coupled inductor as given in Fig. 1 is replaced by the model as shown in Fig. 2. The self-inductances labelled in Fig. 2 as L_1 and L_2 are summation of L_{lk} and L_m . This inductance is measured through a standard open circuit test. The inductance which exists between two magnetically coupled coils is called mutual inductance, labelled as M_{12}. Hence, the model as illustrated in Fig. 2 based on M_{12}, L_1 and L_2 will be used for further analysis. These mutual and self-inductances are the key parameters for defining the design of coupled inductors in the designed tool and simulation.

In [12], the accurate method of series-coupling for calculating the mutual inductance is mentioned. Figure 3 explains it by showing two test circuits, in Fig. 3 (a) where two dots are aligned, and this

configuration is known as directly coupled, differential or series-opposing. The flux generated by two coils connected differentially opposes each other in comparison to series-aiding, cumulative configuration, as shown in Fig. 3 (a) and (b) respectively. The series aiding and opposing inductances L_{opp} and L_{aid} are measured by the test circuits as shown in Fig. 3 are given as:

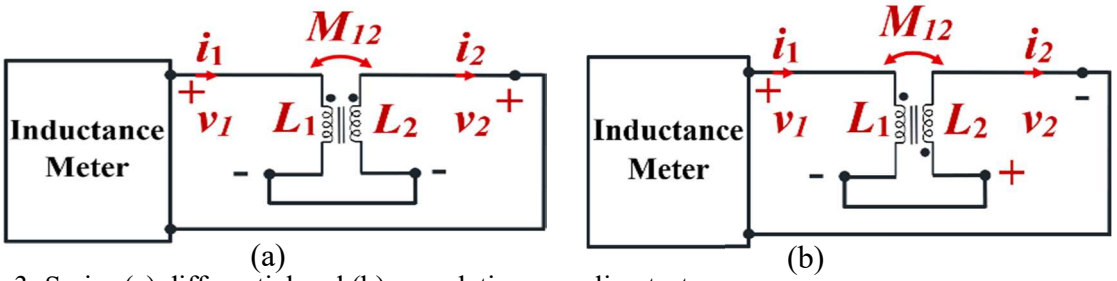

Fig. 3: Series (a) differential and (b) cumulative, coupling test.

$$L_{opp}=L_1+L_2-2M_{12} \quad (1)$$

$$L_{aid}=L_1+L_2+2M_{12}\ , \quad (2)$$

After measuring L_1 and L_2 using open circuit as well as L_{opp} and L_{aid} using series-coupling tests, the mutual inductance can be calculated as follows [11]:

$$M_{12}=\frac{L_{aid}-L_{opp}}{4}\ , \quad (3)$$

The coupling coefficient that is denoted by k relates mutual inductance M_{ji} and self-inductances L_j, L_i of a coupled inductor as given in eq. (6), where k ranges from $-1\leq k\leq 1$.

$$k_{ji}=\frac{M_{ji}}{\sqrt{L_jL_i}} \quad (4)$$

Analysis of a Multiphase Buck Converter with Coupled Inductor

Figure 4 depicts the schematic of a N-phase buck converter that contains a coupled inductor with N number of windings wound on a common core each having self-inductances of L_1, L_2, L_3, ..., L_N. The mutual inductance between the inductors is mentioned as M_{ji}, where I ranges from 1 to N-1 and j ranges from 1 to N. The objective of the following analysis is to investigate the effective inductance and current-slopes of each mode of operation within a switching cycle.

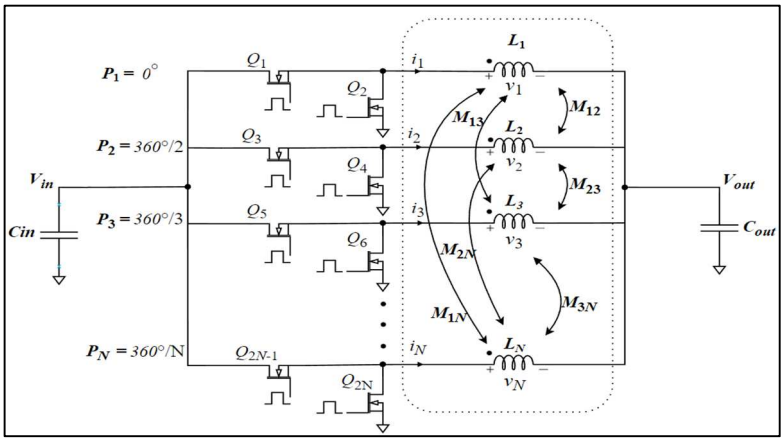

Fig. 4: N-phase buck converter with coupled inductors.

The voltages across the N windings are related to their respective current-slopes as follows:

$$\begin{aligned}
v_1&=L_1\frac{d_{i1}}{dt}+M_{12}\frac{d_{i2}}{dt}+M_{13}\frac{d_{i3}}{dt}+\cdots\cdots\cdots+M_{1N}\frac{d_{iN}}{dt}\\
v_2&=M_{12}\frac{d_{i1}}{dt}+L_2\frac{d_{i2}}{dt}+M_{23}\frac{d_{i3}}{dt}+\cdots\cdots\cdots+M_{2N}\frac{d_{iN}}{dt}\\
&\vdots\qquad\quad\vdots\qquad\quad\vdots\qquad\quad\vdots\\
v_N&=M_{1N}\frac{d_{i1}}{dt}+M_{2N}\frac{d_{i2}}{dt}+M_{3N}\frac{d_{i3}}{dt}+\cdots\cdots\cdots+L_N\frac{d_{iN}}{dt}
\end{aligned} \quad (5)$$

Writing the system of equation, as given in eq. (5), as a matrix yields:

$$\boldsymbol{A}=\begin{bmatrix} L_1 & +M_{12} & +M_{13} & \cdots & \cdots & +M_{1N} \\ +M_{12} & L_2 & +M_{23} & \cdots & \cdots & +M_{2N} \\ +M_{13} & +M_{23} & L_3 & \cdots & \cdots & +M_{3N} \\ \vdots & \vdots & \vdots & \ddots & \ddots & \vdots \\ +M_{1N} & +M_{2N} & +M_{3N} & \cdots & \cdots & L_N \end{bmatrix}, \quad \dot{\boldsymbol{X}}=\begin{bmatrix} {}^{di_1}/_{dt} \\ {}^{di_2}/_{dt} \\ {}^{di_3}/_{dt} \\ \vdots \\ {}^{di_N}/_{dt} \end{bmatrix}, \quad \boldsymbol{B}=\begin{bmatrix} v_1 \\ v_2 \\ v_3 \\ \vdots \\ v_N \end{bmatrix}, \tag{6}$$

To solve the matrix $\dot{\boldsymbol{X}}$ which contains the slope of the currents through each winding of the coupled inductor, the equation as given in eq. (6) can be written as:

$$\dot{\boldsymbol{X}}=\boldsymbol{A}^{-1}.\,\boldsymbol{B}\,, \tag{7}$$

When all the self and mutual inductance values are the same in the inductance matrix A, the situation is referred to as having symmetrical inductance. Other, the situation is called asymmetrical inductance. The inductance matrix must be a singular matrix, which means that the coupling coefficient must be restricted within the range of -1< k <1. The mutual inductances between the windings of the coupled inductor depend upon the direction of the winding; if two corresponding windings have the same direction, as illustrated in Fig. 3, with the dots on the same side, it is indicated by a positive M_{ji} while opposing winding directions are represented by a negative M_{ji} with dots on the opposite sides. Therefore, the direction of each two corresponding windings can easily be entered in matrix $\boldsymbol{A}$ in the presented tool as shown in Fig. 5

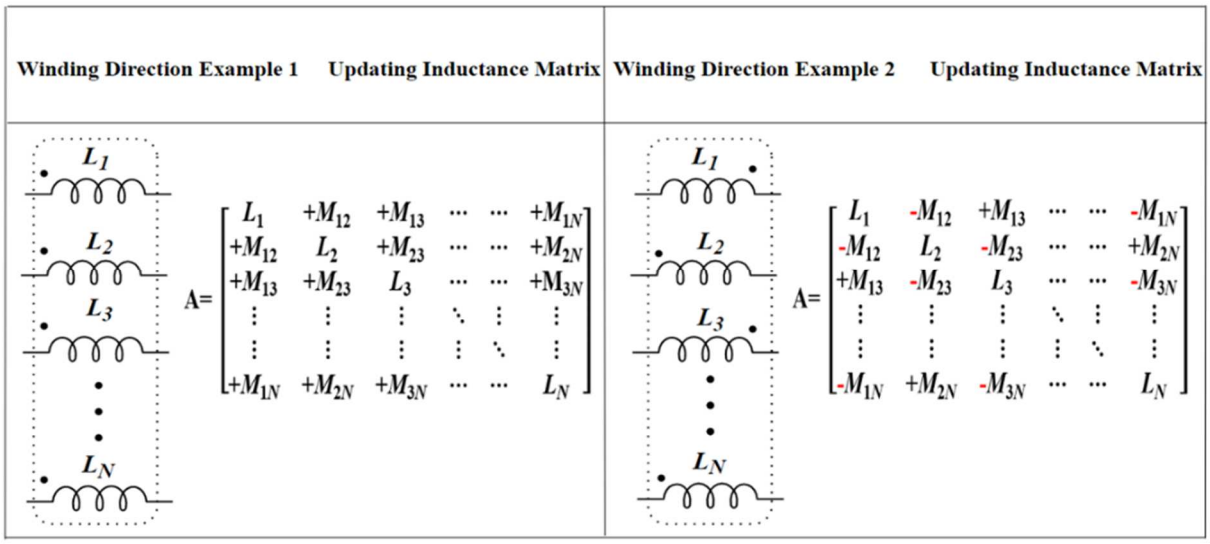

Fig. 5: Changing the winding directions and updating the mutual inductances accordingly in matrices.

The duty cycle range has been divided into different cases, which depend on N. During each case, the voltages across the windings remain the same hence, so do the effective inductances. Within each case, the switching cycle contains N×2 distinct modes or effective inductances. As it can be seen in Fig. 9 and 10, for N = 3, there are six modes such as: m_1, m_2, m_3, …., m_6. Each mode corresponds to a distinct value of effective inductance with its own associated winding current. As N increases, the number of cases increases and the number of effective inductances also increase, indicated in table I. It is worth mentioning here that the analysis was started from N = 2, however; due to space constraints only the relation for N=3 has been mentioned. The effective inductances and slopes of current through the winding have been calculated using the tool, which matches with the results derived manually, as shown in Table II.

Table I: Effectives inductances for $N = 3$ across the whole duty cycle range

Derivation of Effective Inductances Manually			
Modes	**Case 1: $0 < D < 1/3$**	**Case 2: $1/3 \le D < 2/3$**	**Case 3: $2/3 \le D < 1$**
1	$L_{1,C1,m1}=\frac{(L-M)(L+2M)}{L+\left(1+2\frac{D}{D'}\right)M}$	$L_{1,C2,m1}=\frac{(L-M)(L+2M)}{L+\frac{D}{D'}M}$	$L_{1,C3,m1}=L+2M$
2	$L_{2,C1,m2}=L+2M$	$L_{2,C2,m2}=\frac{(L-M)(L+2M)}{L+\left(1+2\frac{D}{D'}\right)M}$	$L_{2,C3,m2}=\frac{(L-M)(L+2M)}{L+\frac{D}{D'}M}$
3	$L_{3,C1,m3}=\frac{(L-M)(L+2M)}{L+\frac{D'}{D}M}$	$L_{3,C2,m3}=\frac{(L-M)(L+2M)}{L+\frac{D}{D'}M}$	$L_{3,C3,m3}=L+2M$
4	$L_{4,C1,m4}=L+2M$	$L_{4,C2,m4}=\frac{(L-M)(L+2M)}{L+\frac{D'}{D}M}$	$L_{4,C3,m4}=\frac{(L-M)(L+2M)}{L+\frac{D}{D'}M}$
5	$L_{5,C1,m5}=\frac{(L-M)(L+2M)}{L+\frac{D'}{D}M}$	$L_{5,C2,m5}=\frac{(L-M)(L+2M)}{L+\left(1+2\frac{D'}{D}\right)M}$	$L_{5,C3,m5}=L+2M$
6	$L_{6,C1,m6}=L+2M$	$L_{6,C2,m6}=\frac{(L-M)(L+2M)}{L+\frac{D'}{D}M}$	$L_{6,C3,m6}=\frac{(L-M)(L+2M)}{L+\left(1+2\frac{D'}{D}\right)M}$

It can be observed from Table II that the derivation of these relations manually is quite time-consuming and prone to error even in the symmetrical design case. Hence, the level of difficulty rises exponentially with asymmetrical inductances and increased number of phases. Therefore, the automation of deriving and solving the above-mentioned relationships is highly advantageous, a task which is addressed by the presented tool.

Development of the Tool

Figure 6 illustrates the flowchart of the presented tool implemented on MATLAB. It starts from taking the user input of the number of phases, *N,* and duty cycle, *D*. Based on the value of *D*, it determines the respective case and initializes the matrix accordingly. It contains the voltages that appear across windings within each mode of switching cycle. With the help of symbolic substitution in MATLAB the respective equations of current-slopes and effective inductances are derived. The tool not only derives all the generalized equations of effective inductances and slopes of all the phase currents but also calculates their numerical values by specifying the input voltage, output voltage and design parameters of the coupled inductor, such as self and mutual inductances.

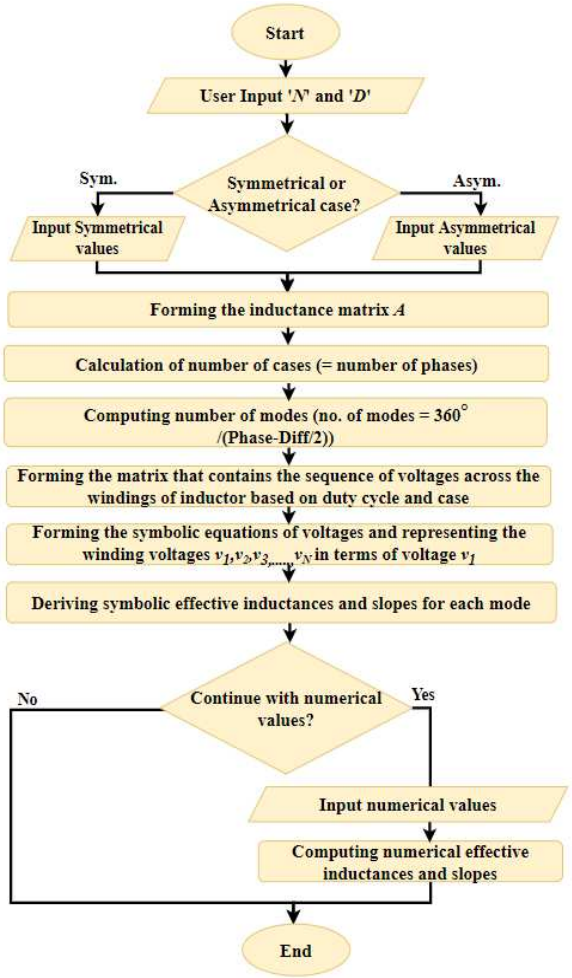

Fig. 6: Flowchart of the presented tool.

It is essential to highlight the fact that available controllers for multiphase converters, used for high performance microprocessors and FPGAs, usually handle up-to 16 phases. In this case, the significance of the presented tool is evident as it automates the analysis of a converter with 16 different cases across the entire duty cycle range. Each case has 32 (=16×2) effective inductances with 512 (=16^2×2) total inductances for the system across the entire range of the duty cycle.

Experimental Validation

For experimental verification of the results, a three-phase buck converter was implemented using a single coupled inductor containing three windings. Figures 7 shows the simplified diagrams of the chosen coupled inductor. They depict the self-inductances L_1, L_2, L_3 and the mutual inductances M_{12}, M_{13}, M_{23} present between the respective windings. Based on the values of self and mutual inductances, which control the coupling coefficients, the coupled inductors are classified into symmetrical and asymmetrical designs.

In Fig. 7 (a), the coupled inductor is designed by interleaving the windings so that homogenous flux can be ensured. Due to interleaving, the distance between windings and core is similar which makes L_{lk} and L_m of three windings uniform. The rod-shaped core makes sure the presence of leakage inductance in the design. Therefore, overall identical values of k exist between windings.

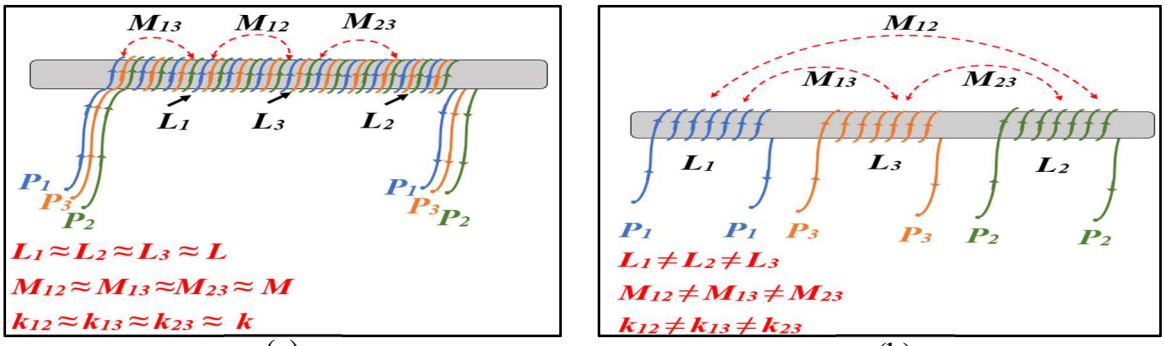

Fig. 7: Simplified diagram of (a) symmetrical and (b) asymmetrical coupled inductor.

The complexity of achieving symmetrical k increases rapidly with the increase in number of phases. It is evident from Table II by looking at design parameters of the symmetrical coupled inductor. The values of self, mutual inductances and coupling coefficients are unequal even for symmetrical design. Therefore, asymmetrical design of coupled inductor is close to practical scenarios. To benchmark the effectiveness of the tool against the design parameters of asymmetrical coupled inductor, such inductor is designed by winding the coils in the manner as explained in Fig. 7 (b). The mismatch in distances between the windings, different numbers of turns, unequal effective core area used by each winding and lack of interleaving while winding the coils all contribute to unequal L_{lk} and L_m. Therefore, the design differs from the symmetrical case due to a mismatch of mutual self-inductances and k. Table II summarizes the design values of symmetrical and asymmetrical coupled inductors measured by the methods mentioned earlier.

Table II: Design parameters of three phase symmetrical and asymmetrical coupled inductors

Design Parameters	Symbols	Symmetrical Design	Asymmetrical Design
Self-Inductances	L_1	4.2540 µH	7.2670 µH
	L_2	4.1660 µH	8.7520 µH
	L_3	4.0320 µH	5.4387 µH
Mutual Inductances	M_{12}	3.3500 µH	3.2004 µH
	M_{13}	2.9790 µH	3.7930 µH
	M_{23}	3.1295 µH	4.2510 µH
Coupling- Coefficient	k_{12}	0.7957	0.4012
	k_{13}	0.7175	0.6005
	k_{23}	0.7654	0.6191

Experimental Setup

The experimental setup consists of three phase buck converter with coupled inductor and their associated controllers. The output of each phase is regulated by a peak current mode controller to guarantee a desired level of accuracy in current sharing as can be seen in Fig. 8.

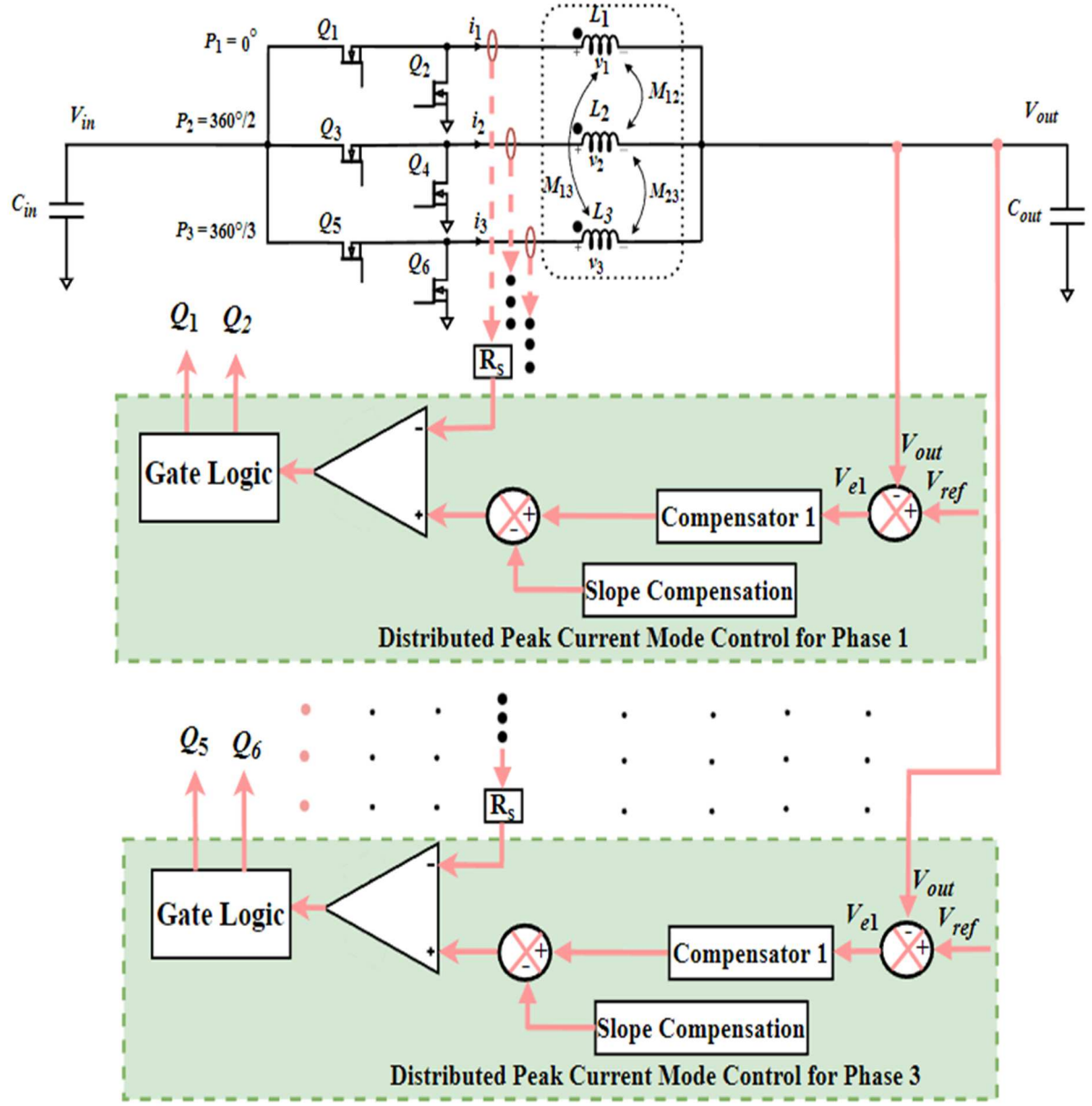

Fig. 8: Block diagram of experimental setup

In Fig. 9(a-c) the inductor currents through each phase of the converter are shown. To benchmark the effectiveness of tool, results from an LTspice simulation and an experimental setup are compared. It can be observed that within each duty-cycle-dependent case, phase currents have similar patterns and rates of change irrespective of their peak values. Due to the phase-shifted control signals, a phase shift of 120º can be seen in phase currents. As the duty cycle changes, the phase current-slopes change accordingly. The current-slopes within each case are highlighted by red dotted lines in Fig. 9 and 10, indicated as m_1, m_2, m_3, …., m_6.

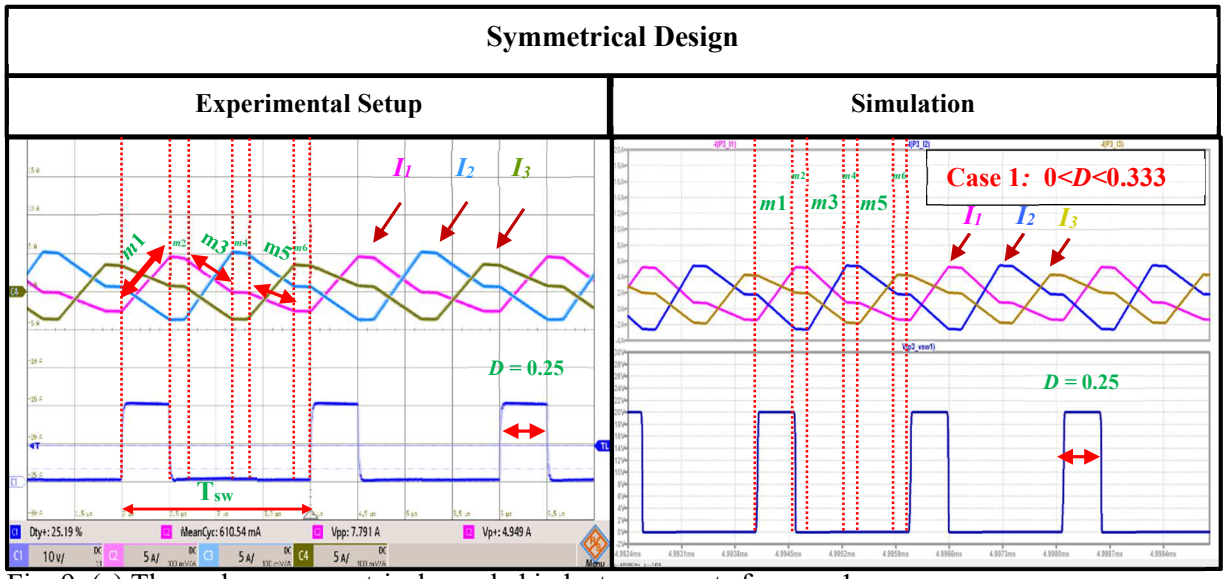

Fig. 9: (a) Three phase symmetrical coupled inductor currents for case 1.

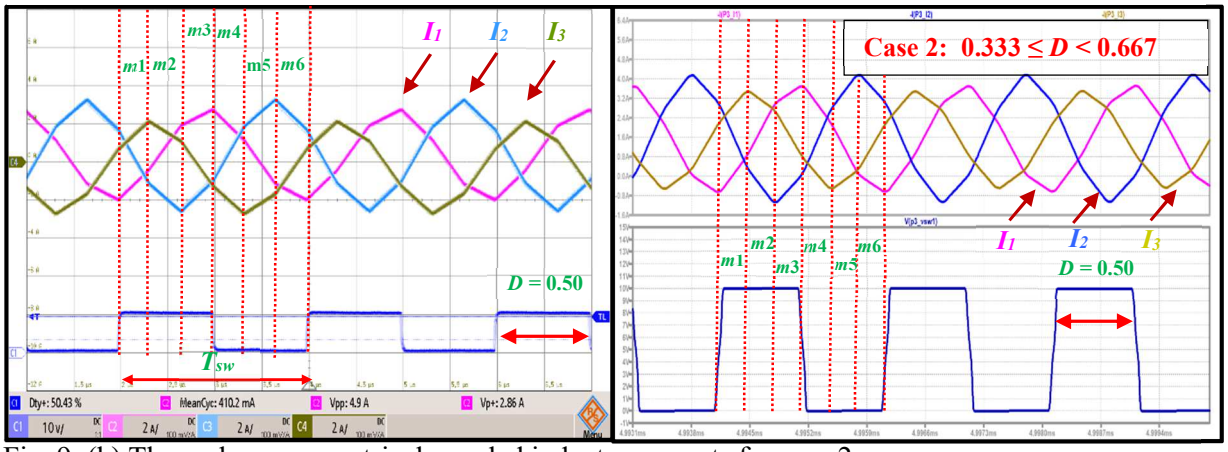

Fig. 9: (b) Three phase symmetrical coupled inductor currents for case 2.

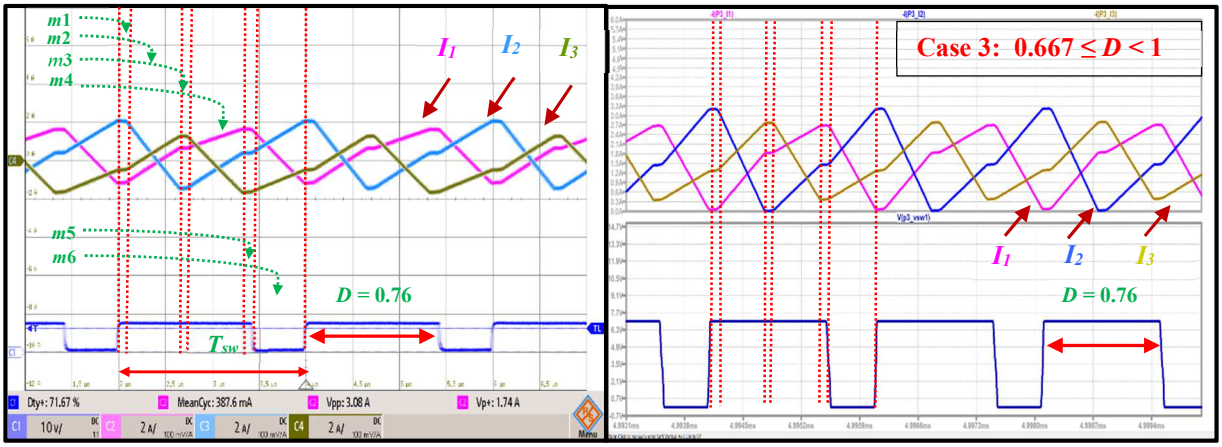

Fig. 9: (c) Three phase symmetrical coupled inductor currents for case 3.

Figure 10 (a-c) shows the operation of the converter with an asymmetrical coupled inductor. The significant difference between Fig. 9 and 10 is that due to the asymmetrical design, the current-slopes, and waveforms of the phase currents in each case have significant disparity than the symmetrical ones. In Fig. 9 (a-c) the phase currents have similar shapes; however, in Fig. 10 (a-c) each phase current waveform has different pattern. Therefore, when analyzing the current-slopes of each case, all the phases must be considered for the asymmetrical design, while in the symmetrical design only phase one is used due to symmetrical slopes of the other two phases.

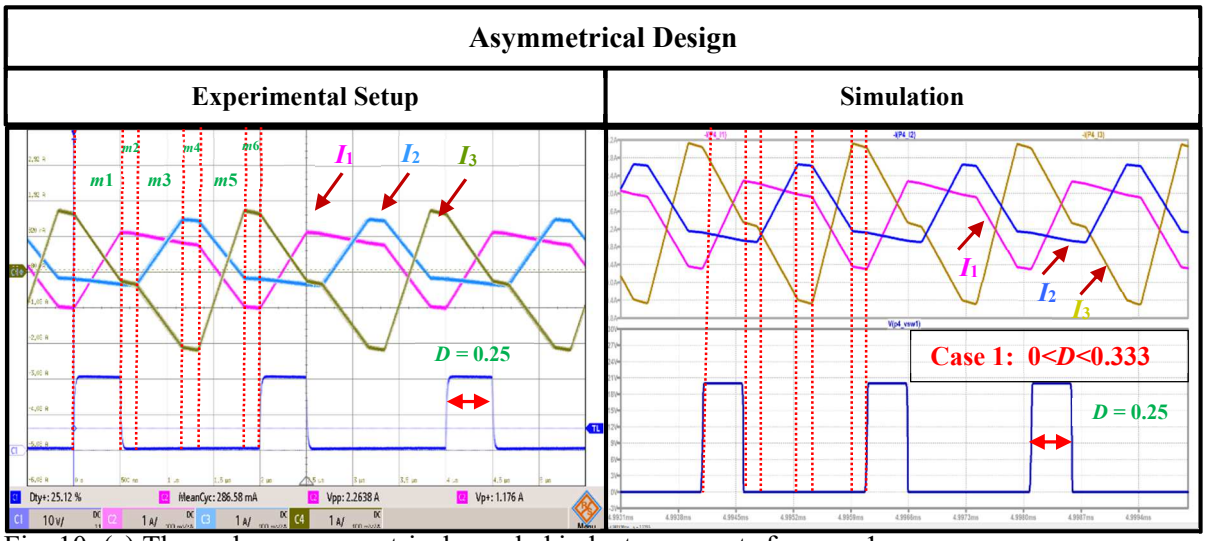

Fig. 10: (a) Three phase asymmetrical coupled inductor currents for case 1

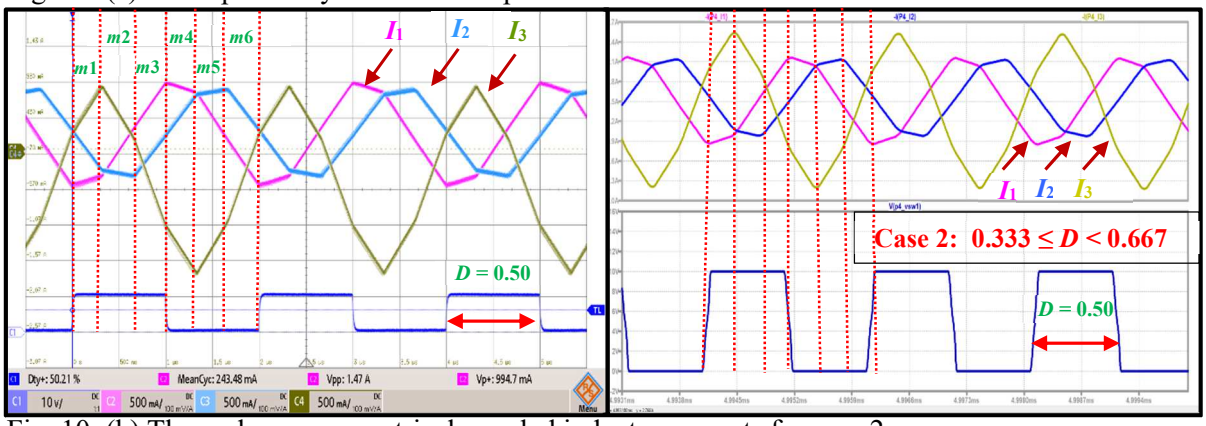

Fig. 10: (b) Three phase asymmetrical coupled inductor currents for case 2

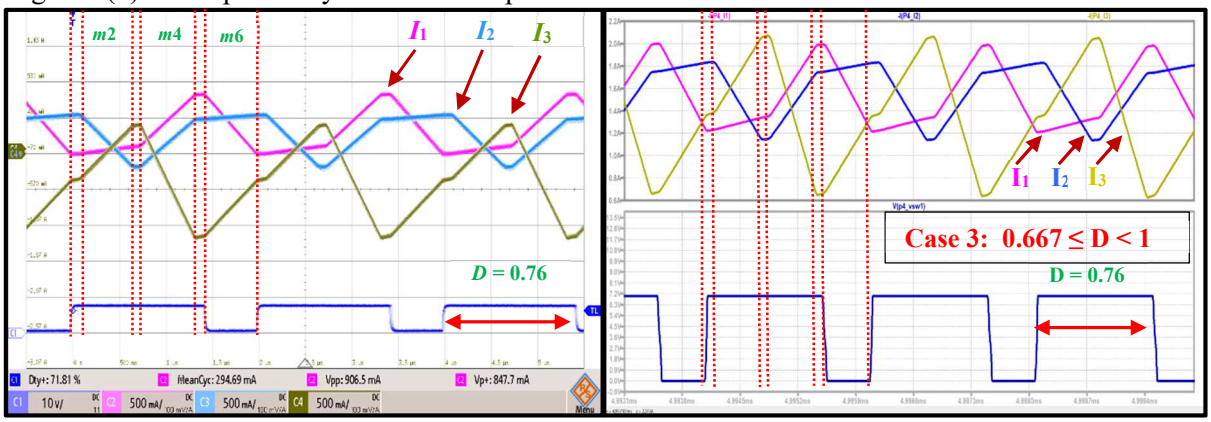

Fig. 10: (c) Three phase asymmetrical coupled inductor currents for case 3.

The accuracy of the presented tool against the simulation and experimental results is benchmarked by observing each slope controlled by its respective effective inductance within a switching cycle as illustrated in Fig. 9 and 10. In Fig. 11, the percentage errors between the simulation-tool, simulation-experimental and tool-experimental setup are presented for symmetrical and asymmetrical coupled inductors. All three phases are analyzed, accounting for the six duty-cycle-dependent modes for the asymmetrical inductor case. Due to the symmetric design of the coupled inductor, only a single phase is presented for comparative analysis. The minimum and maximum percentage error for all the comparison cases ranges from 0.0288 % to 4.661 %. It can be concluded that the error between the tool-experimental setup is more than that of the simulation-tool or the simulation-experimental setup. The reason being that during small periods, measurements of current-slopes can be challenging and prone to inaccuracy

as compared to the period where slope is higher with sharp rise and fall. For instance, high error appears in the asymmetrical design for phase 1 during mode 5 and case 3 where the rate of change of current is not that significant, as can be seen in Fig. 10 (c) and 11. In addition, the root-cause of error also lies in the fact that MOSFETs with parasitic parameters and on-state resistances have been used in the SPICE model. Therefore, due to the voltage drops across the $R_{DS,ON}$ and the voltage across windings, the results are not the same as those found in the theoretical analysis and hardware setup.

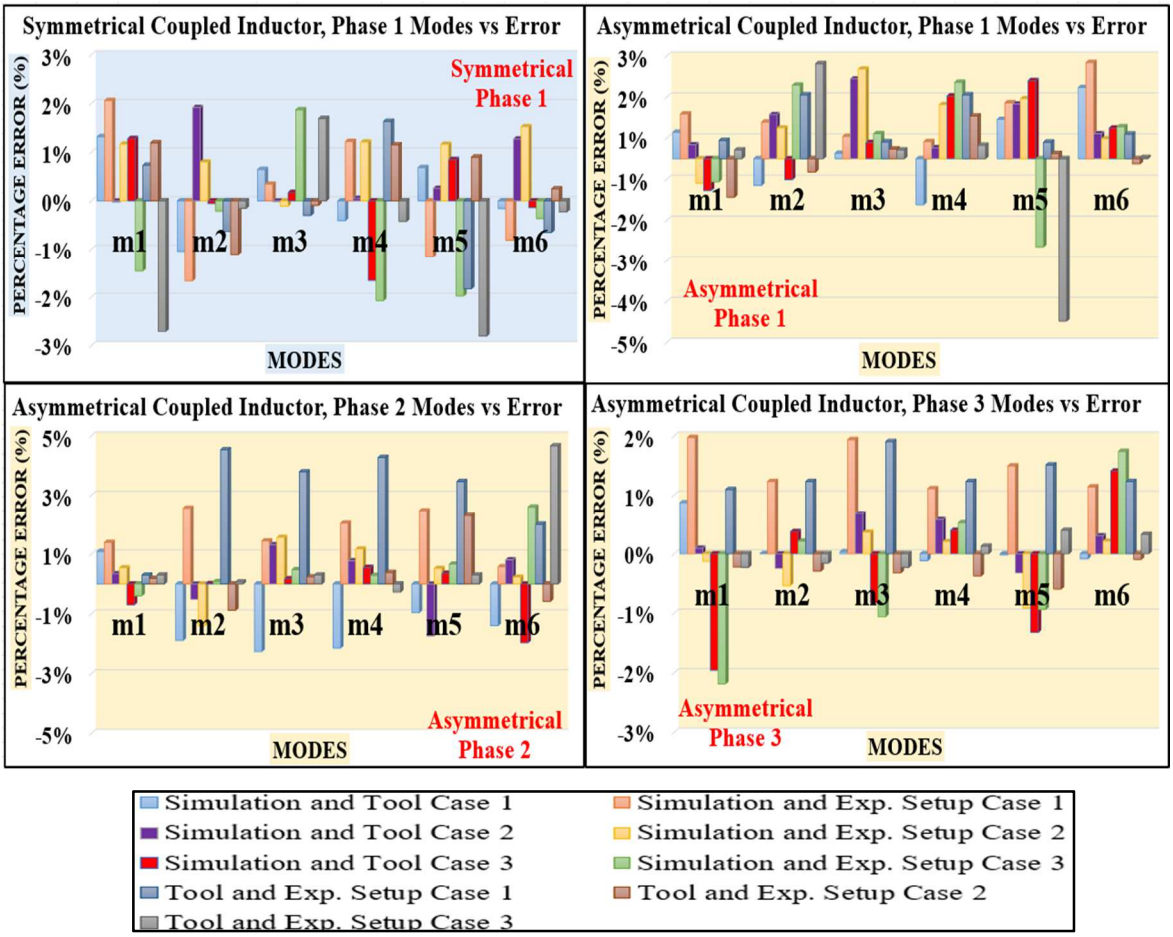

Fig. 11: Comparative analysis of the results of tool, simulation, and experimental setup for symmetrical and asymmetrical designs.

Conclusions

This paper introduces the challenges of analyzing the MPCIBC and proposes a tool to address them. MPBCs, which are widely used in microprocessors and other high-current low-voltage applications, meet the critical efficiency and voltage-regulation requirements by using multiple phases. This paper offers a tool which automates the process of deriving such inductances and current slopes taking into account different design parameter such as inductance symmetry, number of phases and windings direction. The tool produces symbolic representation and values of the effective inductance of each mode of operation in addition to phase current-slopes, which help designers in analyzing and designing the power stage of MPCIBC.

References

[1] Wong PL, Xu P, Yang P, Lee FC.: Performance improvements of interleaving VRMs with coupling inductors, IEEE Transactions on Power Electronics. 2001 Jul;16(4):499-507.

[2] Kroics K.: Design of Interleaved GaN Transistor Based Buck Converter with Directly Coupled Foil Winding Inductor, InCIPS 2020; 11th International Conference on Integrated Power Electronics Systems 2020 Mar 24 (pp. 1-6). VDE.

[3] Wibowo SA, Ting Z, Kono M, Taura T, Kobori Y, Onda KI, Kobayashi H.: Analysis of coupled inductors for low-ripple fast-response buck converter, IEICE transactions on fundamentals of electronics, communications and computer sciences. 2009 Feb 1;92(2):451-5.

[4] Kroics K, BRAZIS US.: Design of coupled inductor for interleaved boost converter, diM. 2014;3(2):2.

[5] Pan T, Wang Y, Qu Z, Tao W.: Topology optimisation and current sharing strategy of interleaved bidirectional dc/dc converter with coupling technique, IET Power Electronics. 2018 Dec;11(15):2470-80.

[6] Lee JP, Cha H, Shin D, Lee KJ, Yoo DW, Yoo JY. Analysis and design of coupled inductors for two-phase interleaved DC-DC converters. Journal of power electronics. 2013;13(3):339-48.

[7] Shi, Meng.: Design and analysis of multiphase DC-DC converters with coupled inductors, PhD diss., Texas A&M University, 2007.

[8] Liu, Jie.: Investigation of Multiphase Power Converter using Integrated Coupled Inductor Regarding Electric Vehicle Application, PhD diss., 2016.

[9] Dong, Yan.: Investigation of multiphase coupled-inductor buck converters in point-of-load applications, PhD diss., Virginia Tech, 2009.

[10] Shi, Meng. "Design and analysis of multiphase DC-DC converters with coupled inductors." PhD diss., Texas A&M University, 2007

[11] Kosai, Hiroyuki, Seana McNeal, Austin Page, Brett Jordan, Jim Scofield, and Biswajit Ray. "Characterizing the effects of inductor coupling on the performance of an interleaved boost converter." *Proc. CARTS USA 2009* (2009): 237-251.

[12] Hayes, John G., Neil o'Donovan, Michael G. Egan, and Terence O'Donnell. "Inductance characterization of high-leakage transformers." In *Eighteenth Annual IEEE Applied Power Electronics Conference and Exposition, 2003. APEC'03.*, vol. 2, pp. 1150-1156. IEEE, 2003